Chapter 3

SIDIS with CLAS12

Chapter 1 introduced polarized Semi-Inclusive Deep Inelastic Scattering (SIDIS) as a powerful tool for investigating the nucleon's internal structure, allowing access to the Transverse-Momentum-Dependent (TMD) distributions. This Chapter aims to outline a preliminary analysis of the Beam-Spin Asymmetry (BSA) associated with the structure-function $F_{LU}^{\sin\phi}$. It is treated as a case study on a possible measurement of non-perturbative QCD phenomena with flavor sensitivity, made possible by having an efficient PID apparatus. The analysis is performed on data acquired by the CLAS12 experiment at JLab, using the first module of the RICH installed in 2018 and refined information from the Pass2 reprocessing of data from periods with Hydrogen (RG-A) and Deuterium (RG-B) unpolarized targets. The second module was not available till the start of experiments with polarized targets in June 2022 whose data were still in the calibration phase at the time of this work. The analysis is based on the efficiency study reported in Chapter 2, which guarantees minimal pion contamination in the eK^+X sample. The study aims to show that it is possible to extract relevant observables with kaons, like the Beam-Spin Asymmetry, despite the reduction in statistics and the limited phase space available with the considered data set. The SIDIS data selection criteria, the analysis method, and the results are included in this Chapter.

3.1 Data

The analyzed data belong to CLAS12 Run Group B (RG-B) and were acquired in the spring of 2019. The target was unpolarized liquid Deuterium, and the longitudinally polarized electron beam was run at $10.6\,\mathrm{GeV}$ and $10.2\,\mathrm{GeV}$ with a current of $50\,\mathrm{nA}$. The average beam polarization was $(84.8 \pm 1.5)\%$; it was monitored during the data-taking period by frequent measurements performed with the Moller polarimeter placed upstream CLAS12. The beam helicity was swapped with a frequency of $30\,\mathrm{Hz}$ to wash out detector effects

and minimize the systematic effects. The torus magnet was full-field *inbending*, pushing positive particles forward outward.

A control sample of data belonging to CLAS12 Run Group A (RG-A) acquired in the spring of 2019 was also used because of the very similar running conditions with respect to Run Group B (RG-B). In this case, the target was unpolarized liquid Hydrogen and the longitudinally polarized electron beam was run at $10.2\,\mathrm{GeV}$ with a current of $50\,\mathrm{nA}$. The average beam polarization was $(84.5 \pm 1.5)\%$. The other conditions were the same.

The analysis is performed on positive kaons: the final state being eK^+X. The standard CLAS12 reconstruction provides the electron identification and the kinematic of the particles, while it is expressly required that the RICH identifies the kaon. These conditions reduce the available statistic because, at the time of data collection, only one of the six CLAS12 sectors was equipped with a RICH module. The analyzed data sample constitutes approximately one-third of the available statistics of electroproduction on Deuterium acquired by RG-B and one-fifth of that on Hydrogen by RG-A.

Most of the focus during the analysis was dedicated to the sample of data provided by RG-B, so generally, the data sample is used to ~~identify data of~~ the scattering of electrons off the Deuterium target.

3.1.1 The CLAS12 SIDIS selection

Electron related cuts

The final states, which include one electron and one positive kaon, are considered in this analysis. For the electron selection, the standard CLAS12 conditions for SIDIS events were applied [43]:

- The electron has to be in the Forward Detector, i.e. its polar angle is between $5°$ and $40°$.

- The electron has to be a trigger particle for the experiment.

- The number of photoelectrons in the HTCC has to be greater than 2.

- The energy in the PCAL has to be greater than $0.07\,\mathrm{GeV}$.

- The DC fiducial cut developed for RG-A is applied (running conditions for RG-B were quite similar, except for the target that was ~~Hydrogen~~ instead of ~~Deuterium~~, so no significant differences are expected).

- The z coordinate of track vertex was selected to be between $-8\,\mathrm{mm}$ and $3\,\mathrm{mm}$.

- The so-called "diagonal cut" is applied for the electron with momentum larger than $4.5\,\mathrm{GeV}$. In this momentum range, the HTCC manifests some inefficiency in distinguishing electron and pion, which can be

mitigated using a selection based on the ratio of the energy deposed in the pre-shower and inner calorimeter.

- The ECAL fiducial cut, which allows to decrease the contamination of negative pion into the electron sample.

Hadron and RICH related cuts

Aiming to study the performance of the RICH, the following conditions were applied to the hadron:

- The particle has to be passed through sector 4 and identified by the RICH;

- Aiming to study the role of the RICH, the momentum is selected to be included in the detector nominal working range $(3 \div 8 \, \text{GeV/c})$;

- The number of photoelectrons in the RICH has to be greater than 2, to well-define the ring.

- The DC fiducial cut developed for RG-A is applied (running conditions for RG-B were quite similar, except for the target that was ~~Hydrogen~~ instead of ~~Deuterium~~, so no significant differences are expected).

- The z coordinate of track vertex is selected to be between $-10 \, \text{mm}$ and $2.5 \, \text{mm}$.

- Having the particle trajectory a key role in the ring reconstruction, which is based on a ray-tracing algorithm, the fitted DC track has to have a reduced $\chi^2_{track} < 8$.

Kinematic cuts

Remembering notation defined for SIDIS in Section 1.3,

$$\ell(l) + N(P) \rightarrow \ell(l') + H(p_H) + X \tag{3.1}$$

where the quantities in parentheses represent the four-momenta, the following quantities can be defined:

- Q is the transferred momentum;

$$Q = \sqrt{(l' - l)^2} = \sqrt{-q^2} \tag{3.2}$$

- y is the fraction of electron energy transferred to the target;

$$y = \frac{P \cdot q}{P \cdot l} \tag{3.3}$$

- W is the center of mass energy

$$W = m_N^2 + 2m_N\nu - Q^2 \tag{3.4}$$

where ν is the energy carried by the virtual photon;

- MM is the missing mass of the reaction

$$MM = \sqrt{(E_{in} - E_{out})^2 - (\mathbf{p}_{in} - \mathbf{p}_{out})^2} \tag{3.5}$$

- z is the fraction of electron energy acquired by the kaon;

$$z = \frac{P \cdot p_H}{P \cdot q} \tag{3.6}$$

- x_F is the so-called Feymann x, the fraction of the nucleon momentum carried by the parton struck by the electron.

$$x_F = \frac{2p_H \cdot q}{Q^2} \tag{3.7}$$

On these quantities, the cuts based on the kinematic were applied:

- $Q^2 > 1\,\mathrm{GeV}^2$, ~~where~~ to exclude the region on which elastic scattering dominates.

- $y < 0.75$, in order to ensure the high virtuality of the photon, limiting the contributions from charge symmetric background.

- $W > 2$, to avoid nuclear resonances with relevant cross-sections.

- $MM > 1.6\,\mathrm{GeV}$, to minimize the contribution of exclusive channels.

- $z > 0.2$, to reduce the probability of hadrons deriving from baryon decays or target fragmentation. In this case, it can be ~~neglected~~ because the requirement on the hadron minimum momentum ~~forces~~ $z > 0.4$

- $x_F > 0.0$, to minimize the effects related to the target fragmentation. In this case, it can be neglected because the high-momentum hadron automatically make the requirement satisfied.

Cuts effect

The effect of cuts is evaluated on the sample of events which include a $3 \div 8\,\mathrm{GeV}$ K^+ identified by the RICH. This means that the used statistics is limited with respect the one available at CLAS12 because the RICH covers[1] one-sixth of the spectrometer.

---

[1] At the time of data taking only one CLAS12 sector was equipped with the RICH

| Selection criteria	Original sample rejection [%]
DC fiducial cut on hadron	52.6
$\chi^2_{track}/NDF < 8$	50.0
y < 0.75	45.6
RICH photons > 3	45.5
$RQ < 0.1$	27.9
Other 11 cuts	$0.1 \div 15$ each
Main 5 cuts combined	93.9
All cuts combined	96.6

Table 3.1: Recap of the percentage of events rejected applying the different selection criteria.

The reduction in statistics produced by each cut was evaluated by applying them separately to the full sample and checking the size of the selected subsample. There are five main cuts, four of them rejecting approximately 50% of the events each and one removing about the 30% of events. Combining these five cuts, the subsample obtained consists of 6.1% of the events. The other selection criteria, separately, rejected events in the range between $0.1 \div 15\%$ of the original sample. Combining all cuts, the final subsample results to be 3.4% of the original sample and is composed of a than 2.5×10^5 events. Table 3.1 contains a recap of the rejection power of the selection criteria. The most effective selections are four related to the hadron and one to the kinematic. In particular, two of them are the conditions described in Section 2.4.2, that are related to the RICH: the request of having at least three photons and the cut on the RQ variable.

The phase space covered by the particles surviving the selection is shown in Figure 3.1, while the distributions as a function of Q^2, x_B, z, p_T are represented in Figure 3.2.

3.2 Analysis

Since the available statistic is limited, the Unbinned Maximum Likelihood (UML) method was selected to obtain the measurement. With respect to the binned method, UML requires more computational resources but provides more reliable results in case of low statistics because it computes the asymmetry term event-by-event instead of using a cumulative histogram. The analysis software was developed by the author using C++ and Clas12root, a framework derived from ROOT CERN that includes methods to read the CLAS12 data files, that are coded in binary HIghly Performance Output (HIPO) format.
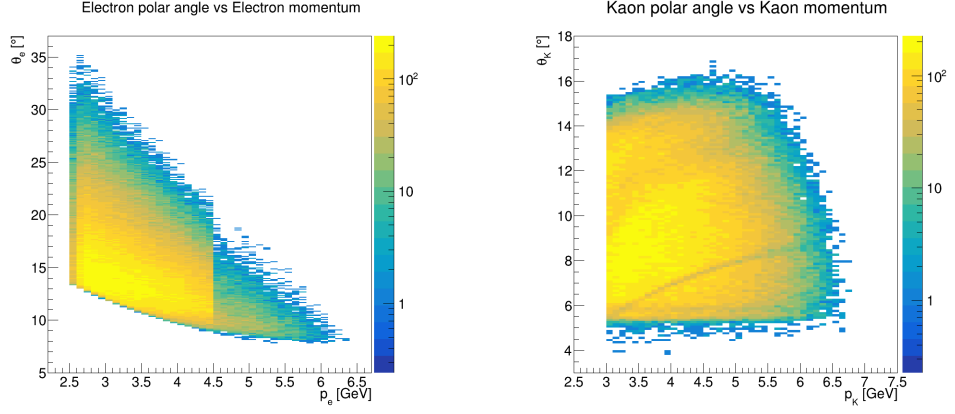
(a) Distribution of the polar angle and momentum of the selected electrons. The separation line visible at 4.5 GeV is due to the "diagonal cut".

(b) Distribution of the polar angle and momentum of the selected kaons. The slightly darker line depends on the small separation between the two regions covered by the aerogel.

Figure 3.1: Phase space covered by the selected events.
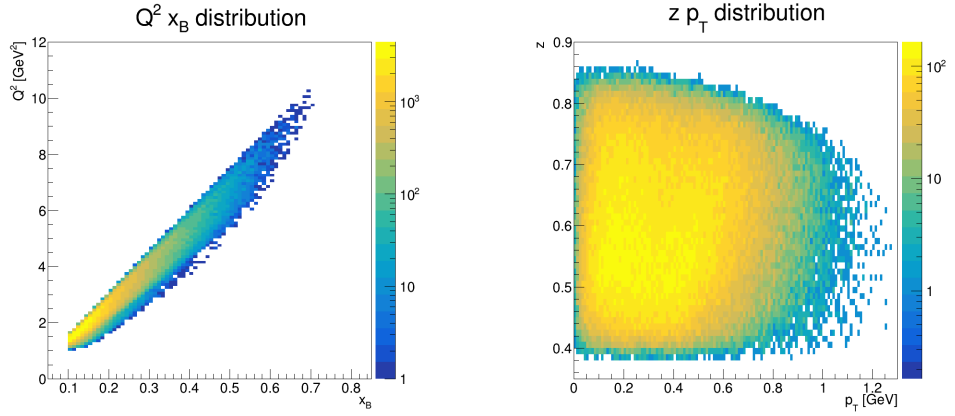
(a) Distribution of events as a function of the Q^2 and x_B variables.

(b) Distribution of events as a function of the z and p_T variables.

Figure 3.2: Distribution of events in the four-dimension of interest.

3.2.1 The Unbinned Maximum Likelihood fit

The UML Fit method is based on the assumption that the Probability Density Function (PDF) associated with the i event has the same functional form of the cross-section

$$PDF(x_i, \alpha) = \frac{\sigma_{UU}(1 + A_i(\alpha))}{\mathcal{N}\left(\int d\sigma_{UU}\right)} \tag{3.8}$$

where x_i is the set of variables associated with the event, α is a set of parameters, $\mathcal{N}$ is a term depending on $\int d\sigma_{UU}$ to normalize the PDF to 1, σ_{UU} is the unpolarized cross-section, and A_i is a term taking into account the wanted asymmetry. If the unpolarized cross-section does not depend on the parameters of the fit, as it happens in this case, the PDF became

$$PDF(x_i, \alpha) = 1 + A_i(\alpha) \tag{3.9}$$

The likelihood function for a set of N independent events can be obtained as

$$\mathcal{L} = \prod_{i=1}^{N} PDF(x_i, \alpha) \tag{3.10}$$

Applying the logarithm to the $\mathcal{L}$ permits the transformation of the product into a sum, making easier the computation:

$$\log \mathcal{L} = \sum_{i}^{N} \log\left[PDF\left(x_i, \alpha\right)\right] \tag{3.11}$$

Under the hypothesis of a large sample of independent measurements, the logarithm of the likelihood behaves like a χ^2.

$$\chi^2 = -2\log\mathcal{L} \tag{3.12}$$

so it is possible to extract the most probable value of the asymmetry by minimizing the χ^2.

To extract the $A_{LU}^{\sin\phi}$ asymmetry, the PDF is

$$PDF_{\pm}(x_i, A_{LU}^{\sin\phi}) = 1 \pm P_b(A_{LU}^{\sin\phi}\sin\phi_i) \tag{3.13}$$

where the sign changes following the helicity of the beam, and P_b is the beam mean polarization. This PDF is automatically normalized, so it can be used directly in the definition of the likelihood

$$\log\mathcal{L} = \sum_{i}^{N^+ + N^-} \log\left[1 \pm P_b\left(A_{LU}^{\sin\phi}\sin\phi_i\right)\right] \tag{3.14}$$

The $F_{LU}^{\sin\phi}$ term is related to the BSA $A_{LU}^{\sin\phi}$ by the equation

$$A_{LU}^{\sin\phi} = \frac{\sqrt{2\varepsilon(1-\varepsilon)}F_{LU}^{\sin\phi}}{F_{UU}} \tag{3.15}$$

where ε is a kinematic factor defined in Equation 1.12. Then, the likelihood is

$$\log \mathcal{L} = \sum_i^{N^+ + N^-} \log \left[1 \pm P_b \left(\frac{\sqrt{2\varepsilon(1-\varepsilon)} F_{LU}^{\sin\phi}}{F_{UU}} \sin\phi_i \right) \right] \qquad (3.16)$$

and it is sufficient to minimize $-2\mathcal{L}$ to find the value of the structure-function ratio.

This method has the advantage of being independent of the binning in ϕ and provides results also if applied to relatively small samples. However, the UML method requires large computation resources to perform the minimization over thousands of events, and it is not always easy to define the PDF and its normalization. In the case of the extraction of $F_{LU}^{\sin\phi}$ for kaon, the advantages appeared more relevant than the disadvantages, so the UML was selected.

3.2.2 UML fit validation

The UML fit was implemented using the ROOT::Math::Minimizer class, which allows the minimization of a function depending on one or more parameters. The software was validated on the $e\pi^+ X$ data acquired during Run Group A (RG-A), in the same experimental configuration of RG-B but using Hydrogen instead of Deuterium as a target. To validate the analysis, the structure-function ratio $\frac{F_{LU}^{\sin\phi}}{F_{UU}}$ is extracted as a one-dimensional function of x_B, z, and p_T and compared with the published result [35]. The validation process was performed using the baseline CLAS12 reconstruction software, excluding the RICH, to have the same phase space of the original analysis. The comparison of the results is shown in Figures 3.3a, 3.3b, and 3.3c. Despite the plots suggest a non-uniform systematic difference between the UML and published results, the trend of the functions is the same. The discrepancy is likely due to differences in the event selection of the two samples of pions. To validate this idea, a comparison between UML and binned fit was applied to the sample selected by the author, obtaining similar results. The plots are shown in Figure 3.4. Indeed, a small systematic difference is visible between the two methods. In principle, the UML fit should be more reliable because it does not suffer the binning effects. In any case, a systematic related to the extraction method was evaluated and described in the following. ~~The implementation of the UML method is considered completed and the latter was~~ used to obtain any other results shown in the following.
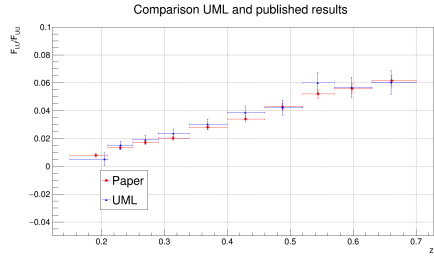
3.3 Systematic errors

The discussion of the systematic errors is still partially incomplete because the analysis ~~started~~ a few months before writing this document. ~~It happened because~~ the new version of the CLAS12 reconstruction software, the so-called
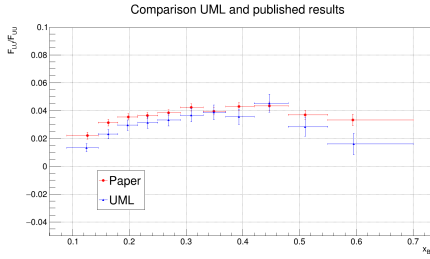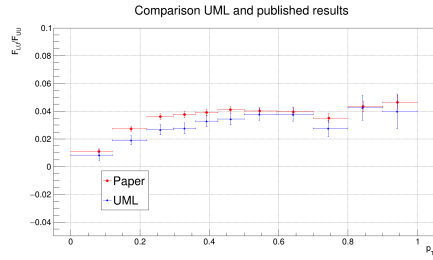
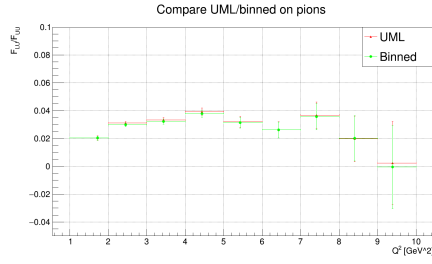**(a)** Comparison as a function of x_B.

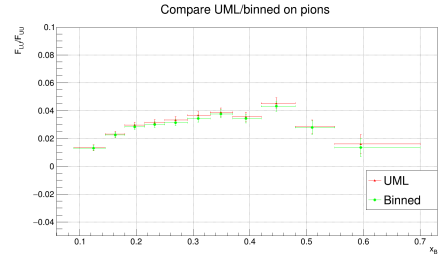**(b)** Comparison as a function of z.
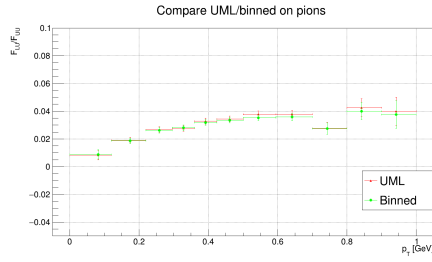

(c) Comparison as a function of p_T.

Figure 3.3: One-dimensional comparisons of the $\frac{F_{LU}^{\sin\phi}}{F_{UU}}$ obtained by the UML fit and published results on pion data. The plots show a systematic difference between the two analyses. The one-dimensional plot as a function of Q^2 was not shown because it was not inserted in the Reference [35].
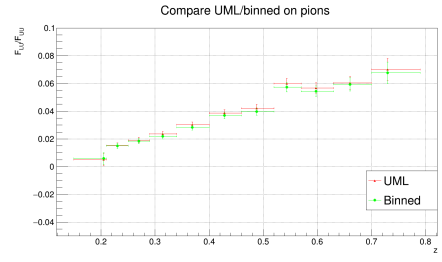
63

(a) Comparison as a function of Q^2.

(b) Comparison as a function of x_B.

(c) Comparison as a function of p_T.

(d) Comparison as a function of z.

Figure 3.4: Comparisons between the $\frac{F_{LU}^{\sin\phi}}{F_{UU}}$ obtained by the UML fit and the binned fit as one-dimensional function in electron and hadron variables. The results were computed on the same sample of pions obtained using the baseline CLAS12 software. A small systematic difference is observed.

Pass2, became available only after Summer 2023. Moreover, the CLAS12 simulation still does not include ~~the RICH detector~~, making the estimation of the systematics more complex. In any case, the present results focus on a subsample of the RICH data and are limited in statistical precision. A detailed systematic evaluation is not essential at this stage and will be evolved as needed. The systematic related to CLAS12 were derived from internal documents of the collaboration [44] and from the Reference reporting the CLAS12 results of pion BSA [35], ~~having evaluated their values as reasonable and~~ being the two SIDIS analyses the same except for the selected hadron. The systematic related to the identification of the kaon, which is related to the main subject of this thesis, was evaluated by exploiting the results of the pion contamination on the kaon sample study described in Section 2.4.

3.3.1 Main systematic uncertainties from CLAS12 measurements

Beam polarization uncertainty

The beam polarization was approximately weekly measured during the CLAS12 data taking. The measurements were performed using a Moller polarimeter, with a typical systematic error of 2%. This value has to be added in quadrature to the corresponding statistical error computed for the data sample considered. The statistical uncertainty associated with the RG-B data was 1.5%. The total uncertainty on the beam polarization is therefore

$$p_b = (84.8 \pm (stat)1.5 \pm (sys)2.0)\% = (84.8 \pm 2.5)\%. \qquad (3.17)$$

The relative uncertainty on the beam polarization is used to define the correspondent systematic uncertainty on the structure-functions ratio:

$$\frac{\delta \frac{F_{LU}}{F_{UU}}}{\frac{F_{LU}}{F_{UU}}} = \frac{\delta A_{LU}^{\sin\phi}}{A_{LU}^{\sin\phi}} = \frac{\delta BSA}{BSA} = \frac{\delta p_b}{p_b} = 2.9\% \qquad (3.18)$$

Acceptance and bin migration effects

The acceptance effects should be studied using the Monte Carlo (MC) by introducing a controlled asymmetry and comparing the structure-function ratio obtained using the generated and reconstructed particle by the simulation. This study could not be carried out because the RICH volume is not yet available in the CLAS12 MC. It is assumed that the estimation made for the pion cases can be a reasonable value, that can be used for this preliminary analysis. Because the two analyses are performed on different phase spaces, the relative uncertainty is increased by a factor of 2 as a safety margin. The relative uncertainty in the pion cases was set to 2.7%, ~~than it~~ is set to ~~the~~ 5.4% for kaon study.

Radiative effects

The emission of a radiative photon in the scattering process introduces a mismatch between the virtual photon energy and the reconstructed value, this causes a bias on the SIDIS kinematic. Currently, there are no tools available to accurately estimate radiative effects for SIDIS BSA. The cuts on y and on MM, combined with the accessible values of z and p_T, minimize the contaminations from the radiative tail of exclusive events. Moreover, the radiative effects are expected to be small in SIDIS processes thanks to the requirement of at least one hadron in the final state. For the case of pion, an estimation of the upper limit of the effect was performed using the dedicated software, setting this value at 3%. The analogous study for kaon is formally missing, but ~~a similar effect is expected~~; thus, for this preliminary study, the value estimated for pion was used.

Effects of fiducial cuts

The same fiducial cuts were applied to both the helicity states, and this effect was expected to be small. The main effect is related to the fiducial cut applied to the PCAL. By comparing the structure-function ratio for $e\pi^+X$ obtained by applying the loose and the medium cuts, as shown in Figure 3.5, the difference was found to be always less than the 5% and compatible with 0. As a consequence, this effect is neglected.

### PID electron systematic effect

A possible source of systematic is the misidentification of negative pions as electrons. The diagonal and the ECAL fiducial cut reduce contamination to about 2%. The systematic uncertainty associated with the pion contamination into the electron sample can be estimated with the MC. It is assumed that the effect is largely independent of the positive hadron particle and, therefore, can be used for this preliminary kaon analysis. The relative uncertainty, as a function of x_B, Q^2, z, and p_T is shown in Figure 3.6. The effect is always comparable with zero, then it is neglected.

### Extraction method systematic effect

Despite the previous consideration of expecting the UML fit theoretically better than the binned fit, it was decided to evaluate a systematic uncertainty depending on the extraction method, in case something in the implementation was not working as expected. For this reason, the systematic uncertainty was evaluated using the pion sample, which has larger statistics, to minimize the ~~bins' effect on the binned method.~~ The uncertainties were estimated from the ~~plots like the one~~ shown in Figure 3.4b. The ~~plots of the~~ difference between the ~~two~~ ~~methods results~~ were fitted using a linear ~~function~~. This allows the
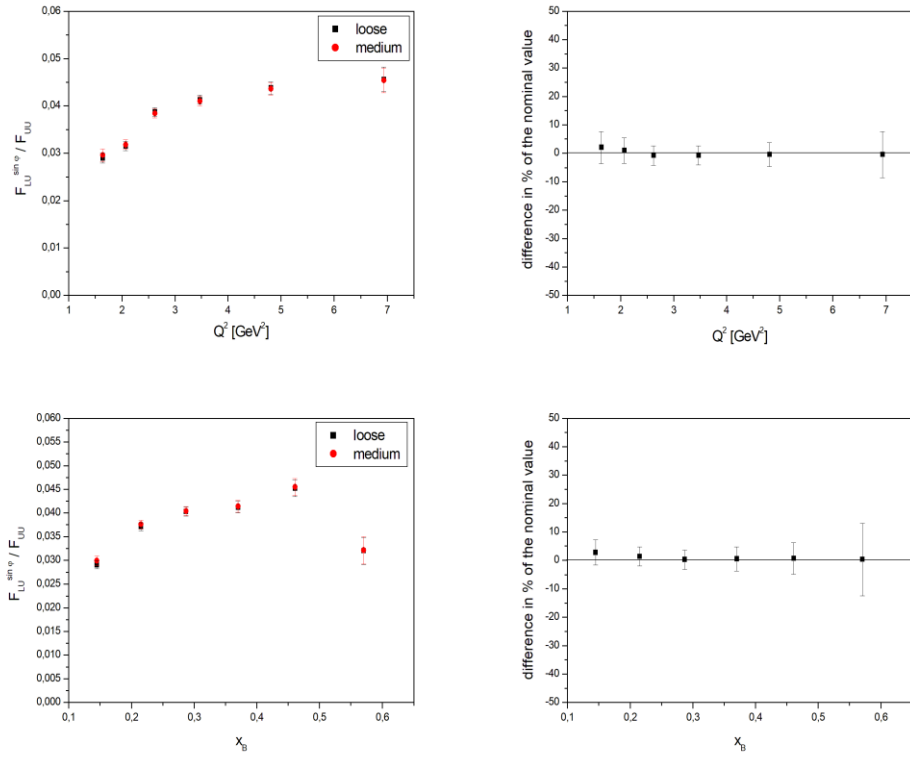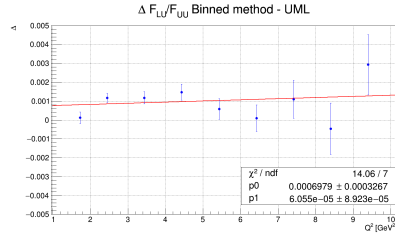
Figure 3.5: Plots describing the study on the effect the PCAL fiducial cut, taken from the CLAS12 RG-A common analysis note [44].
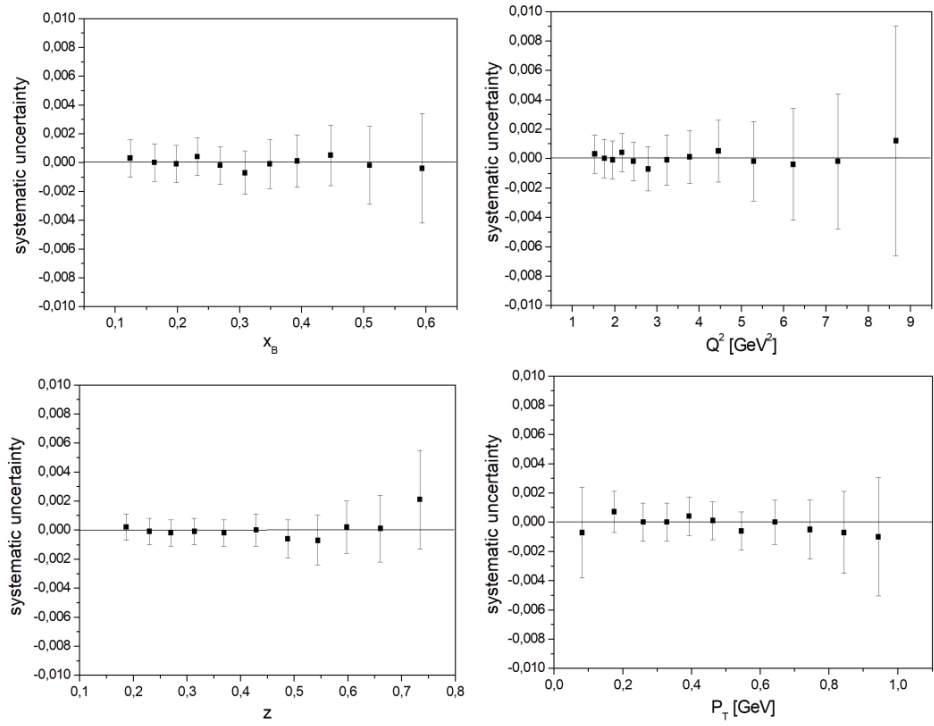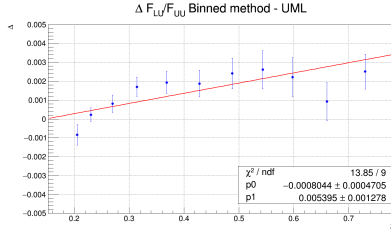
Figure 3.6: Systematic uncertainty associated with the π^- contamination into the e^- sample, taken from the CLAS12 RG-A common analysis note [44].
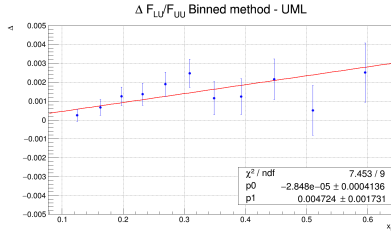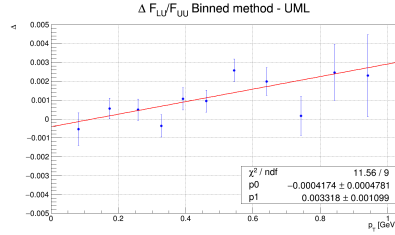
(a) Difference between UML and binned extraction results as a function of x_B.

(b) Difference between UML and binned extraction results as a function of Q^2.

(c) Difference between UML and binned extraction results as a function of z.

(d) Difference between UML and binned extraction results as a function of p_T.

Figure 3.7: Estimation of the systematic uncertainties related to the results extraction method.

estimation of a constant term and ~~possibly~~ dependence on the ~~variables~~. The linear function describing the systematic uncertainty are shown in Figure 3.7. The found values of the parameters p_0 and p_1 allow us to neglect this source of systematic uncertainty.

3.3.2 Systematic uncertainty caused by the kaon sample contamination

The systematic uncertainty on the structure-function ratio caused by the π^+ ~~contaminating~~ the K^+ sample was evaluated by exploiting the results ~~on kaon sample contamination provided by~~ the study described in Section 2.4. The effect of pion contamination on the structure-function ratio (the ratio with F_{UU} is implicit) can be described by using:

$$F_{LU}^{meas} = F_{LU}^K + \delta F_{LU}^{cont} = F_{LU}^K + \left(\frac{N_\pi}{N_K} \Delta_{F_{LU}} \right) \qquad (3.19)$$

where N_π is the number of pions contaminating the kaon sample, N_K is the number of kaons constituting the sample after removing the contamination, and $\Delta_{F_{LU}}$ is the difference between the structure-function obtained ~~by measuring it whit~~ pion or kaon SIDIS

$$\Delta_{F_{LU}} = F_{LU}^\pi - F_{LU}^K. \qquad (3.20)$$

Because in this analysis the statistical error is ~~still the main relevant~~, it was decided to estimate an upper limit to this systematic uncertainty by a~~pproximating~~ $\Delta_{F_{LU}} \simeq F_{LU}^{\pi}$.

The F_{LU}^{π} used to evaluate the systematic was obtained from the $e\pi^{+}X$ events satisfying the same selection criteria applied to the kaon sample; in particular, the pion was recognized by the RICH. These selection criteria were determined to select a comparable phase space. The plots showing the systematic uncertainty as a one-dimensional function were fitted with a first-order polynomial to highlight trends. The linear function was used to estimate punctually the systematic uncertainty. The systematic as a one-dimensional function of the electron and hadron variables are reported in Figures 3.8a, 3.8b, 3.8c, and 3.8d.

In the four-dimensional analysis, the uncertainty derived from PID was estimated ~~by evaluating it~~ using the one-dimensional functions ~~and~~ the mean value of the corresponding variable computed for the bin and averaging over the four dimensions. The systematic uncertainty on the structure-function ratio associated with the contamination of kaons from pion is included in the range between 0.0005 and 0.002, at least one order of magnitude less the current statistical uncertainty. This fact ~~confirmed the possibility~~ of using the upper limits obtained identifying ΔF_{LU} ~~as~~ the structure-function obtained from pion. Being this systematic effect small, it was simply introduced in the global uncertainty of the measurement without applying a specific correction.

3.3.3   Global systematic uncertainty

The global systematic uncertainty is computed by adding all the sources of systematic uncertainty in quadrature. Table 3.2 recaps the results described previously. The relative systematic uncertainty introduced by the non-RICH related sources is evaluated to be 6.7%. In the analysis, the systematic derived from the pion contamination in the kaon sample depends on the electrons and hadron variables, so it is computed specifically for each bin. It ~~assumes~~ absolute values between 0.0005 and 0.002, resulting comparable with the other systematic sources. The systematic uncertainties are found to be smaller ~~rather~~ than the statistical error, which is, as expected, the dominating source of uncertainty in this analysis. For this reason, a correction of the systematics effect was not developed, but they were simply added in quadrature to the statistical component.
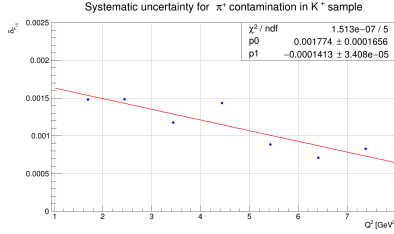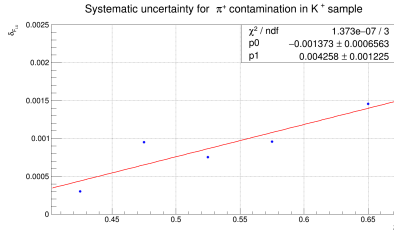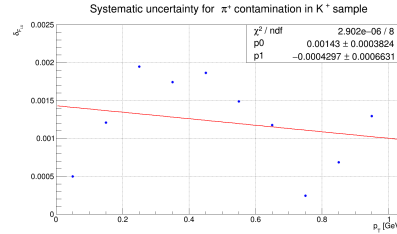
(a) Relative uncertainty associated with pion contamination into kaon sample.
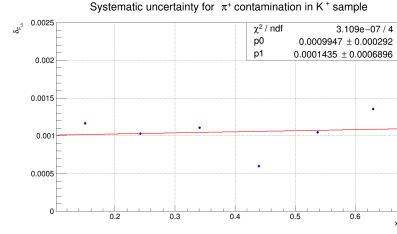
(b) Relative uncertainty associated with pion contamination into kaon sample.

**(c)** Relative uncertainty associated with pion contamination into kaon sample.

(d) Relative uncertainty associated with pion contamination into kaon sample.

Figure 3.8: Estimation of the PID systematic uncertainties related to the pion contamination into the kaon sample.

Uncertainty source	Average relative systematic uncertainty
Beam polarization	2.9%
Acceptance and bin migration	5.2%
Radiative effects	3.0%
Fiducial cuts	$\sim 0.0\%$
π^- contamination on e^-	$\sim 0.0\%$
Results extraction method	$\sim 0.0\%$
Systematic excluding RICH	6.7%

Table 3.2: Recap of the contribution to the systematic uncertainty.
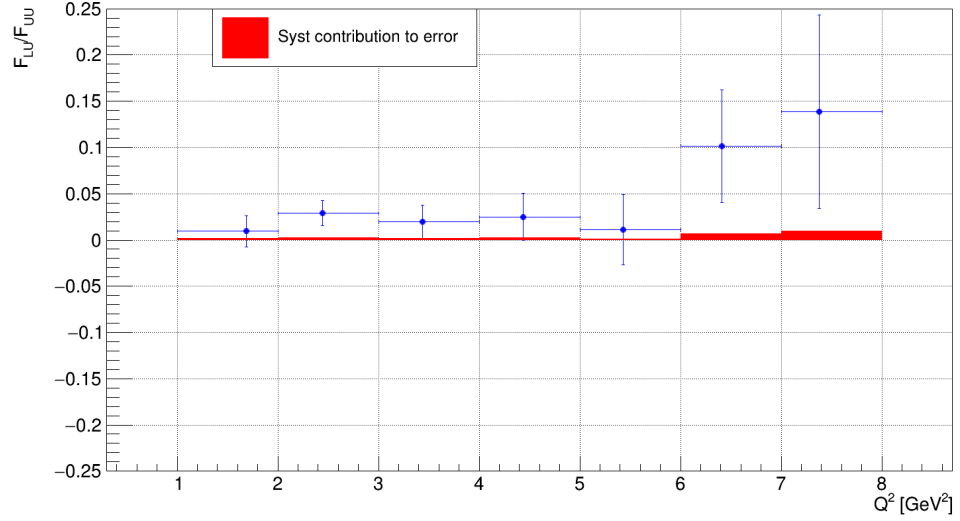
Figure 3.9: $F_{LU}^{\sin\phi}/F_{UU}$ as a function of Q^2. The red area shows the contribution of the total systematic uncertainty to the measurement error.

## 3.4 Results

The analysis is still partially incomplete because the Pass2 data became available only after summer 2023[2]. However, the aim of this study was to show that the BSA exists for kaons and it is detectable at CLAS12, and that an efficient PID identification based on RICH introduces only a minor systematic uncertainty on the measurement. An analogous analysis was performed on data taken from CLAS12 RG-A, which ran the experiment in the same configuration of RG-B but using a Hydrogen instead of Deuterium target. The results from RG-A data are shown in Appendix A.

3.4.1 One-dimensional results

The one-dimensional results are shown as a function of the relevant electron and kaon variables in Figures 3.9, 3.10, 3.11, and 3.12. They show that the asymmetry is detectable using the CLAS12 spectrometer for kaons identified by the RICH. The red area indicates the total systematic uncertainty, which is a second-order effect with respect to the statistical uncertainty. Despite the limited statistical precision, the plots show the asymmetry tends to zero for vanishing z and p_T, as expected from theory.

---

[2]The work will not remain unfinished. It was not possible to complete it before the end of the Ph.D., but the author will continue to work with the CLAS12 data and conclude the analysis, aiming to achieve a publication.
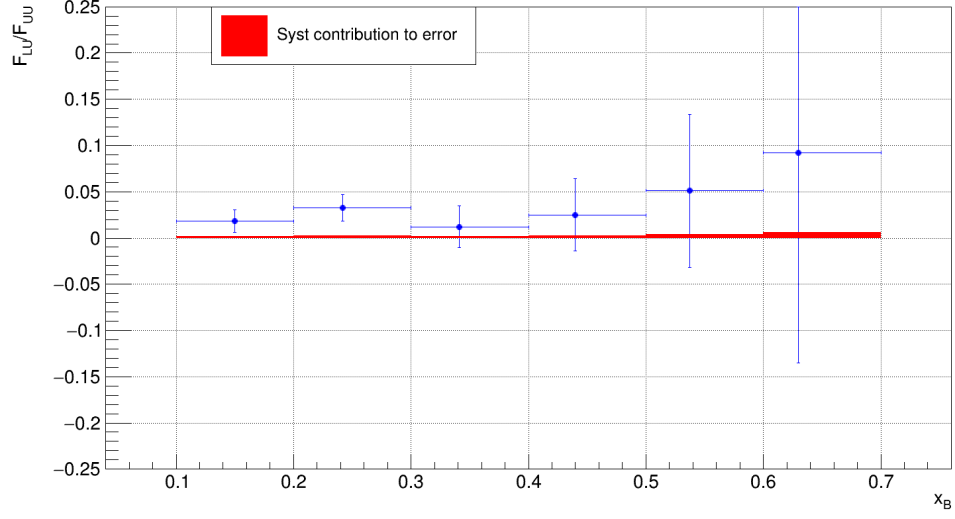
Figure 3.10: $F_{LU}^{\sin\phi}/F_{UU}$ as a function of x_B. The red area shows the contribution of the total systematic uncertainty to the measurement error.
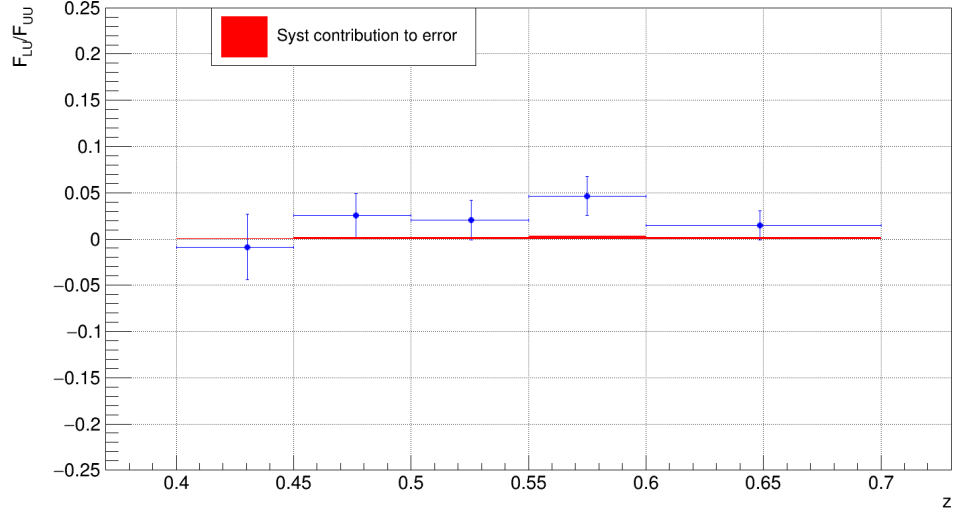
Figure 3.11: $F_{LU}^{\sin\phi}/F_{UU}$ as a function of z. The red area shows the contribution of the total systematic uncertainty to the measurement error.
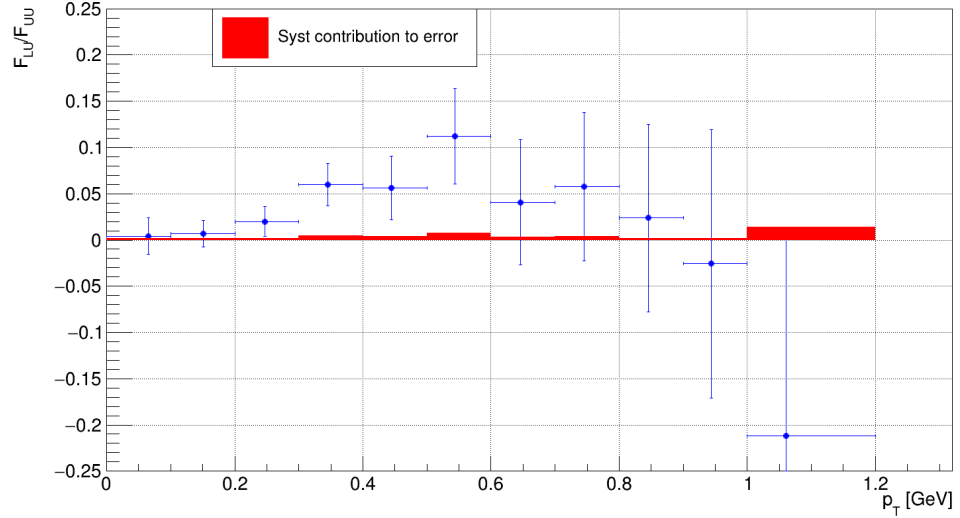
Figure 3.12: $F_{LU}^{\sin\phi}/F_{UU}$ as a function of p_T. The red area shows the contribution of the total systematic uncertainty to the measurement error.

3.4.2 Four-dimensional results

A four-dimensional binning was applied to the kaon sample because multidimensional analysis can provide useful information to constrain the theoretical models. The binning procedure was made in two steps: first, the sample is divided into three bins of the electrons' kinematical variables, which are represented in Figure 3.13a, and second, each of them is divided into four or six bins in the hadron variables, as shown in Figures 3.13b, 3.13c, and 3.13d. The main criteria were to maximize the number of bins but maintain sufficient statistics in the order of $\sim 10^4$ events-per-bin.

The results as a function of p_T for each bin in the electron variables and hadron z are shown in Figures 3.14, 3.15, and 3.16. The plots show a behavior more consistent with theory for higher Q^2 bins, where the asymmetry tends to zero for small p_T and z, but the statistical error remains large. Increasing the statistics and the phase space in the future will provide possibilities to make more definitive conclusions.

3.4.3 Comparison between pion and kaon

It is possible to compare the $F_{LU}^{\sin\phi}$ structure-function obtained from SIDIS pion and kaon. The pion sample was selected, requiring the hadron to be identified by the RICH to obtain a phase space comparable with the kaon sample. All the selection criteria previously described for the kaon sample were applied to the pion sample.
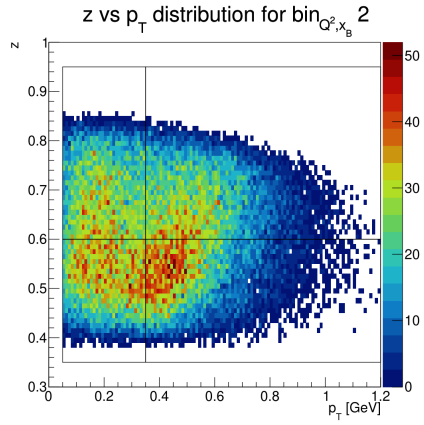
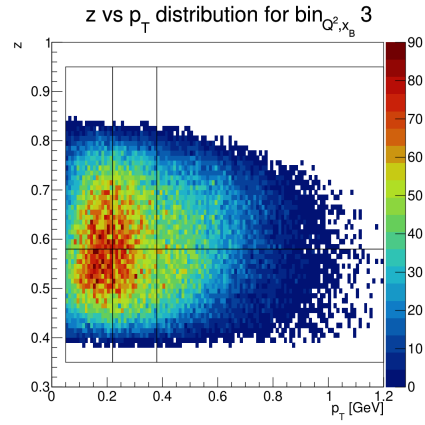The one-dimensional comparison of the structure-function obtained from
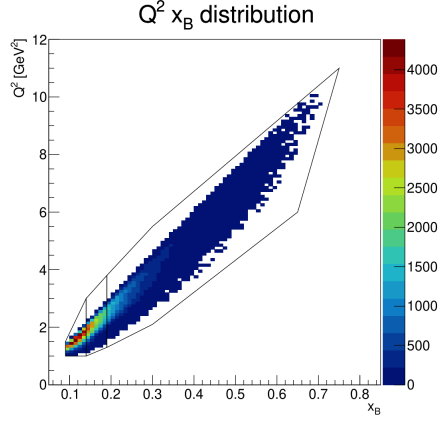
(a) Binning applied to the Q^2, x_B variables for kaons.
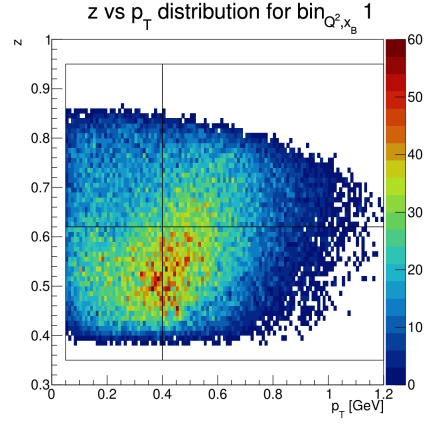
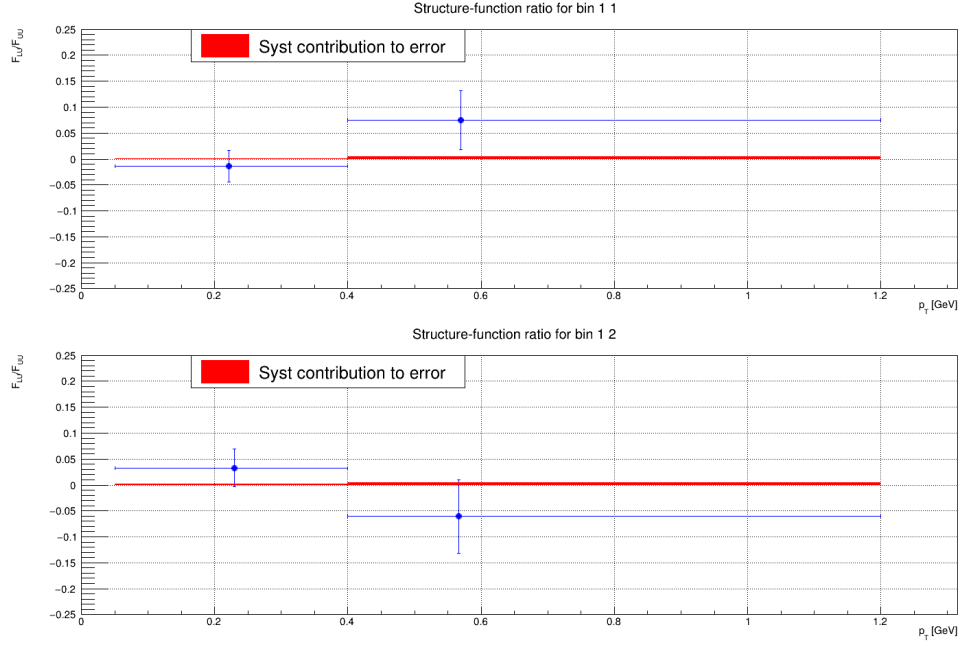**(b)** Binning applied to the z, p_T variables for the first bin of Q^2, x_B.

(c) Binning applied to the z, p_T variables for the second bin of Q^2, x_B.
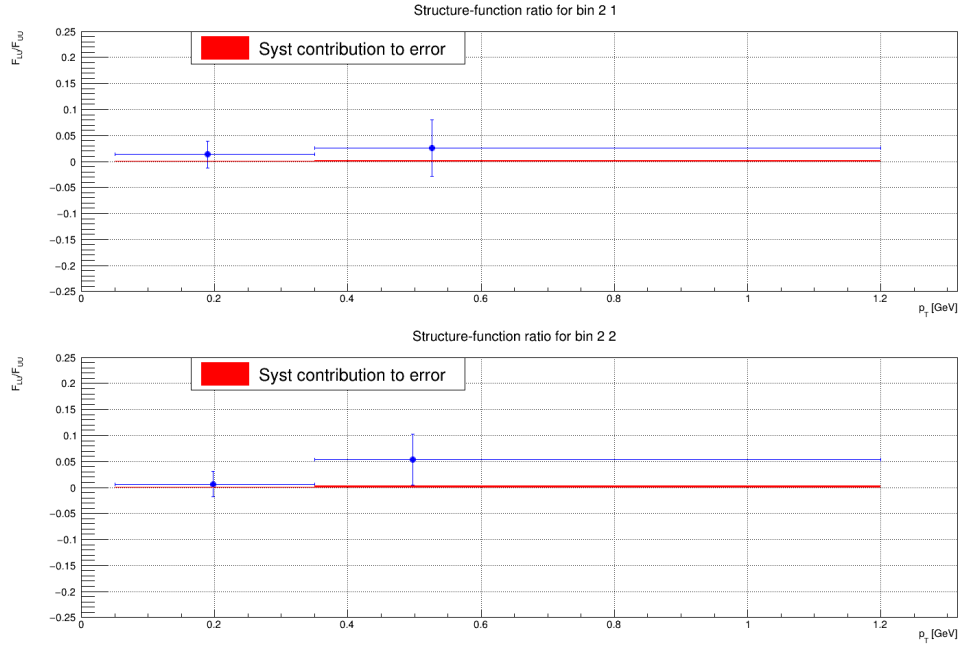
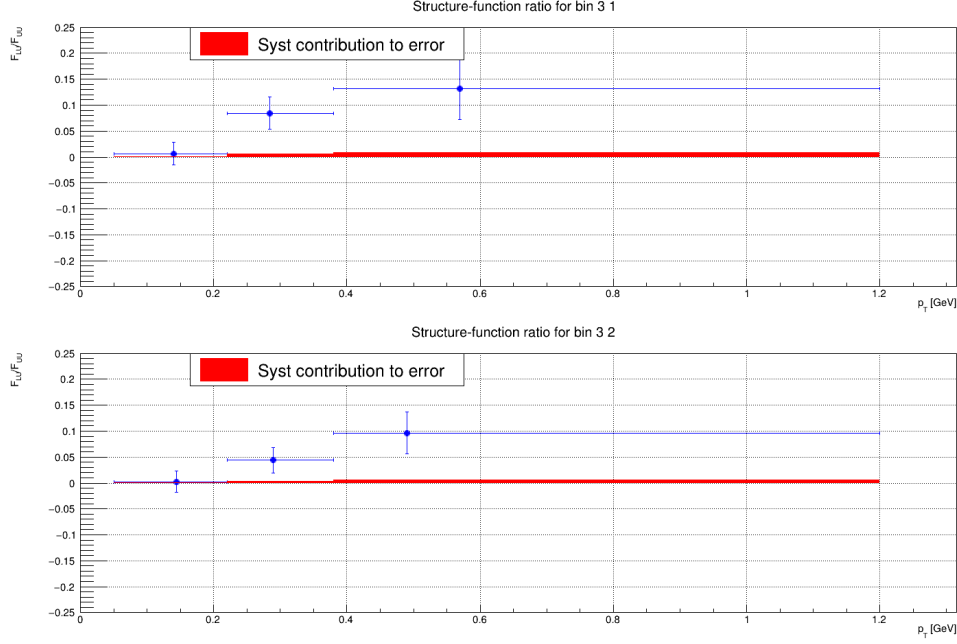**(d)** Binning applied to the z, p_T variables for the third bin of Q^2, x_B.

Figure 3.13: Distribution of events in the four-dimension of interest.

Figure 3.14: $F_{LU}^{\sin\phi}$ as a function of p_T, for the first bin on the electron variables and the two bins in z.

Figure 3.15: $F_{LU}^{\sin\phi}$ as a function of p_T, for the second bin on the electron variables and the two bins in z.

Figure 3.16: $F_{LU}^{\sin\phi}$ as a function of p_T, for the third bin on the electron variables and the two bins in z.
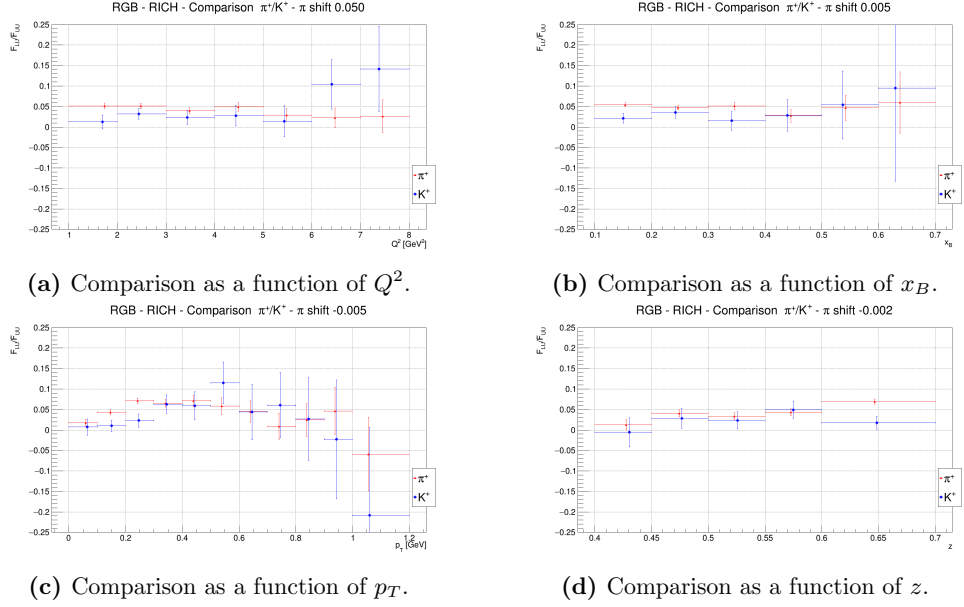
pion and kaon is shown in Figure 3.17. Generally, the results obtained from analyzing the two samples are close, but especially the kaons are dominated by the statistical uncertainty. More reliable results could be obtained in future studies with the completion of the RICH alignment extending the accessible angle range up to the design value of 26° and analyzing the full statistics.

3.4.4 Comparison with literature results

A preliminary comparison with results available in literature was done with HERMES measurement from Reference [45] and COMPASS measurement from Reference [46]. The results from HERMES are specifically obtained from kaon SIDIS, while COMPASS published results of positive mixed hadrons.

The mean values of kinematic variables are reported in Figures 3.18, 3.20, and 3.22. They show the capability of CLAS12 to extend the phase space to a higher x_B region. The kinematic regions are not ~~easyly~~ comparable, and more interesting information shall be available once the CLAS12 multi-dimensional analysis will be completed by running over all the available statistics and extending the kinematic region covered by the RICH when the software alignment will be completed.

The structure-function comparison are shown in Figure 3.19, 3.21, and

(a) Comparison as a function of Q^2.

(b) Comparison as a function of x_B.

(c) Comparison as a function of p_T.

(d) Comparison as a function of z.

Figure 3.17: $F_{LU}^{\sin\phi}/F_{UU}$ obtained from pion and kaon samples identified by the RICH. The points for pion are slightly shifted along the x-axis to not overlap the error bars

3.23. Despite all the limitations of the present analysis, CLAS12 results are comparable with the measurement of HERMES and COMPASS, and for several bins, show that the high-luminosity of CLAS12 allows a reduction of the statistical error. The addition of the second RICH module is expected to further reduce the impact of statistical error on kaon SIDIS measurement, allowing to obtain high-precision information to constraint theoretical models.

3.4.5 Future SIDIS studies using the CLAS12 RICH

This Chapter showed that from CLAS12 data it is possible to extract beam spin-asymmetries for SIDIS kaon despite the limited statistics analyzed. In the immediate future, the analysis will be extended to the full sample of recorded data on Deuterium, including several runs acquired with the torus in opposite polarization and more favorable for positive hadron acceptance. Moreover, the completion of the RICH alignment, made possible with the Pass2 reconstruction software, will permit to almost double the phase space covered up to the design value of 26° in polar angle. To ultimate the measurement, the data for kaons with momentum lower than 3 GeV, identified by the standard CLAS12 PID, can be included to further extend the phase space. The addition of the second module of the detector, which occurred in 2022, will increase the available statistics, allowing us to divide the data in more dense bins, providing more information to constrain the TMDs.
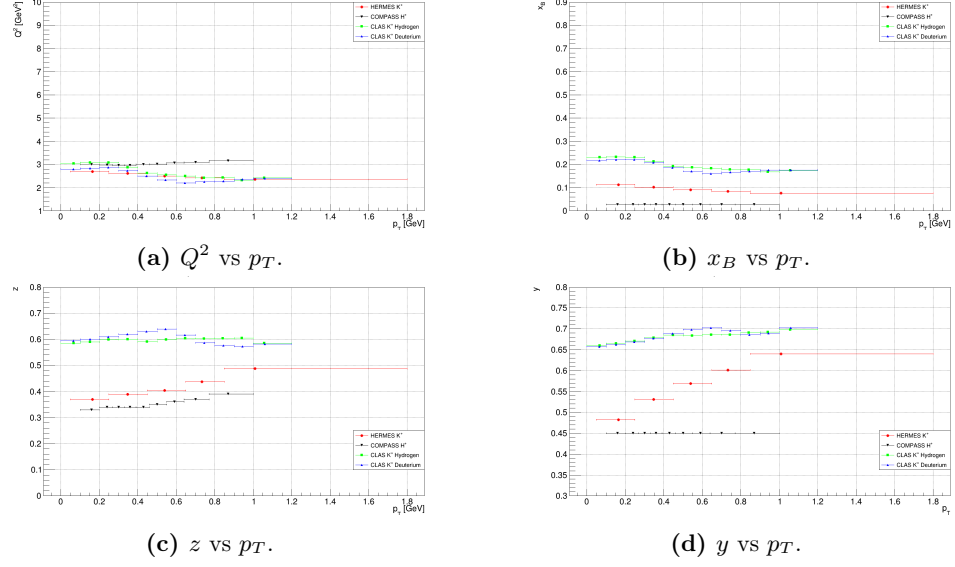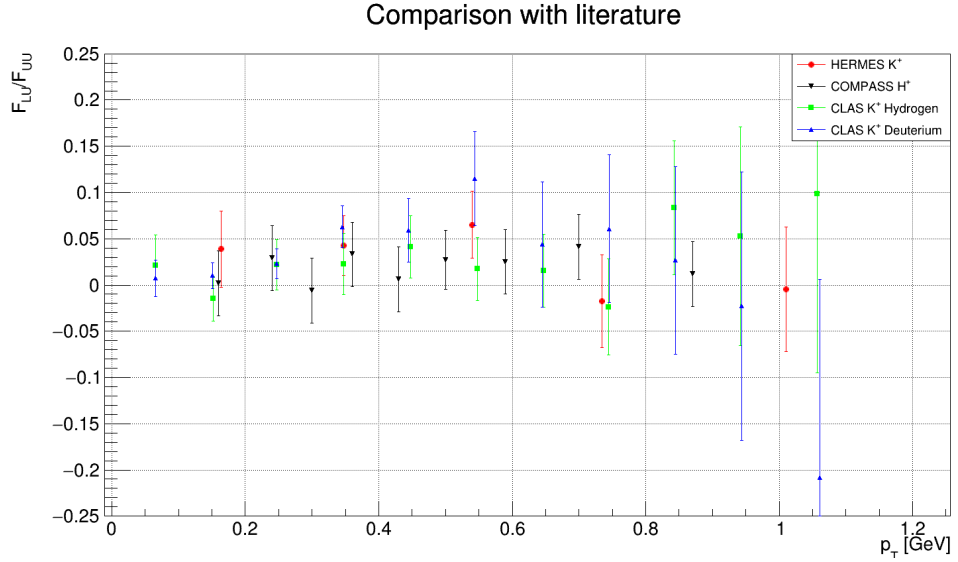
(a) Q^2 vs x_B.

(b) p_T vs x_B.

(c) z vs x_B.

(d) y vs x_B.
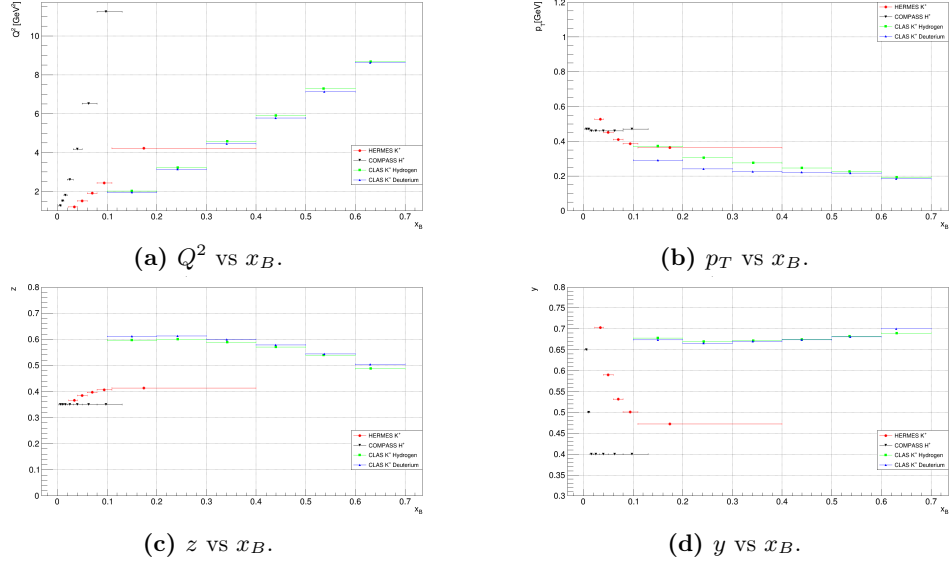
Figure 3.18: Trends of the kinematic variables Q^2, p_T, z, and y as a function of x_B for the results of experiments COMPASS, HERMES, and CLAS12. The y-axes of the plots are extended at least to the values achievable with CLAS12.
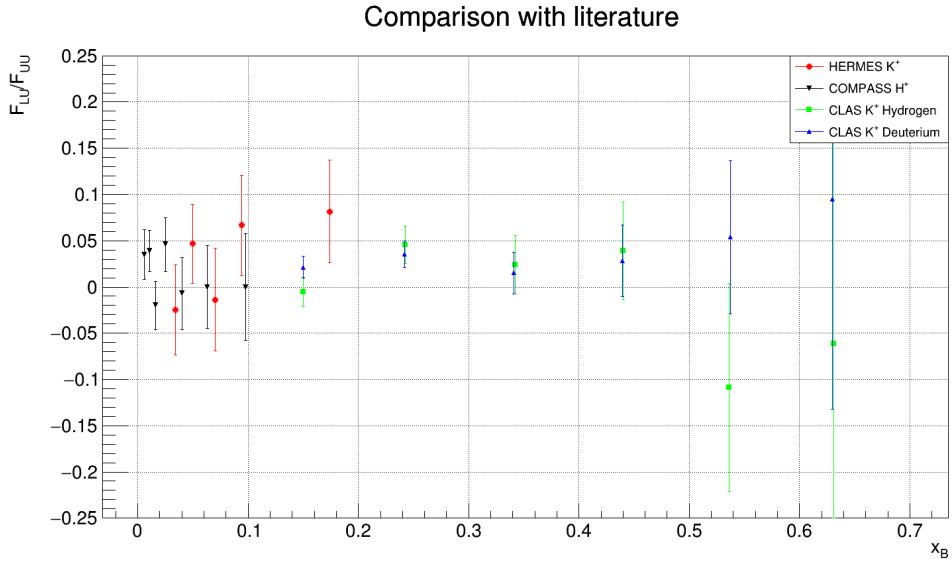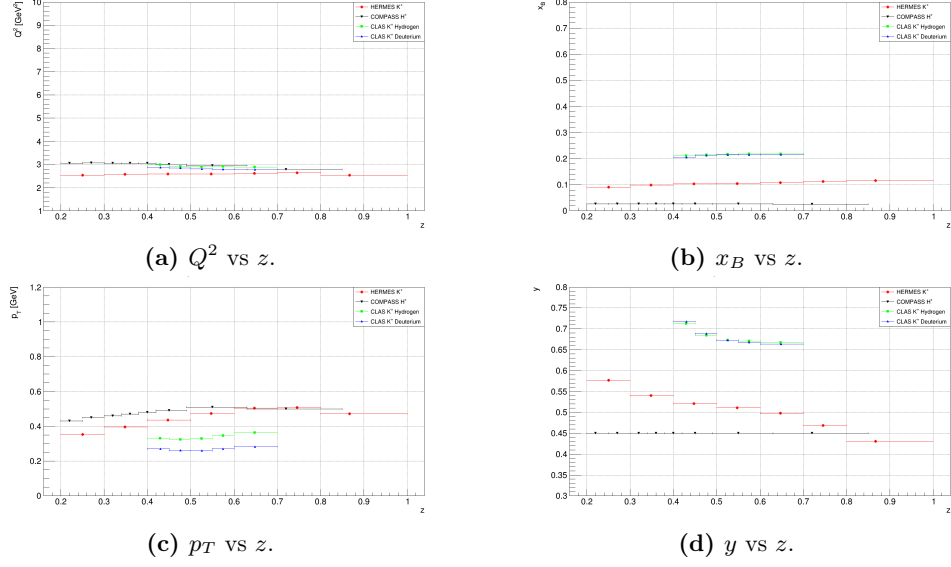

Figure 3.19: Structure-function measured from COMPASS positive mixed hadrons data [46], HERMES K^+ data [45], and CLAS12 RG-A and RG-B K^+ data, expressed as a function of x_B. The bin width bars were removed to make the plot more readable; they are the same as shown in Figure 3.18.

79

(a) Q^2 vs p_T.

**(b)** x_B vs p_T.

(c) z vs p_T.

(d) y vs p_T.

Figure 3.20: Trends of the kinematic variables Q^2, x_B, z, and y as a function of p_T for the results of experiments COMPASS, HERMES, and CLAS12. The y-axes of the plots are extended at least to the values achievable with CLAS12.

Figure 3.21: Structure-function measured from COMPASS positive mixed hadrons data [46], HERMES K^+ data [45], and CLAS12 RG-A and RG-B K^+ data, expressed as a function of p_T. The bin width bars were removed to make the plot more readable; they are the same as shown in Figure 3.20.

80

(a) Q^2 vs z.

(b) x_B vs z.

(c) p_T vs z.

(d) y vs z.

Figure 3.22: Trends of the kinematic variables Q^2, x_B, p_T, and y as a function of z for the results of experiments COMPASS, HERMES, and CLAS12. The y-axes of the plots are extended at least to the values achievable with CLAS12.
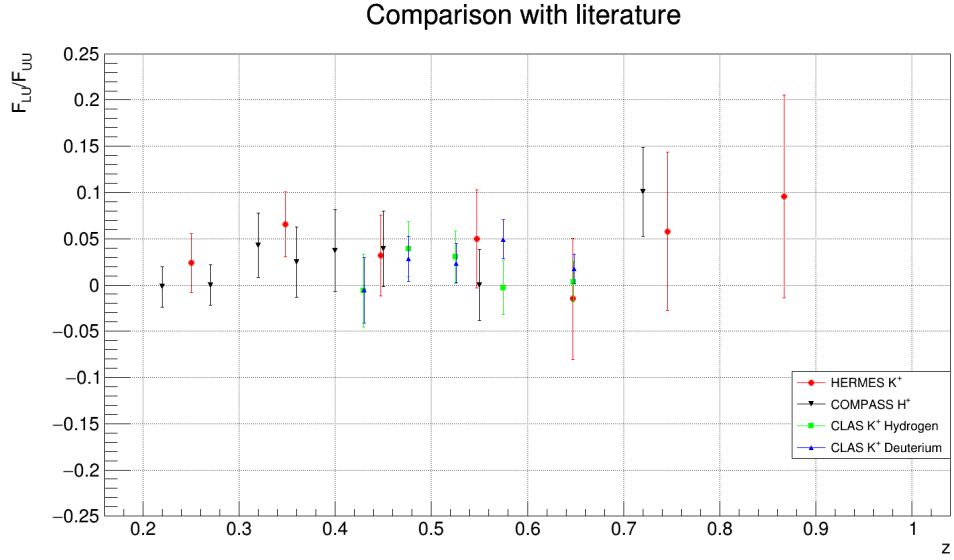
Figure 3.23: Structure-function measured from COMPASS positive mixed hadrons data [46], HERMES K^+ data [45], and CLAS12 RG-A and RG-B K^+ data, expressed as a function of z. The bin width bars were removed to make the plot more readable; they are the same as shown in Figure 3.22.

81

This study demonstrates the capability of the RICH to efficiently identify hadrons in the high-momentum range of CLAS12, between $3\,\mathrm{GeV/c}$ and $8\,\mathrm{GeV/c}$. RICH information will help several studies that are ongoing on kaons, like the measurement of other terms of the SIDIS cross-section or the dihadron spin-asymmetries including at least one kaon. Moreover, the study of the high-momentum SIDIS kaons provides access to the high z region, and to the possibility of ancillary investigations, for example, about the role of vector mesons.